DOI: 10.24352/UB.OVGU-2017-081 TECHNISCHE MECHANIK, 37, 1, (2017), 48-61
submitted: March 6, 2017

Lengthwise Fracture of Two-Dimensional Functionally Graded Non-Linear Elastic Beam

V. Rizov

Non-linear elastic analysis of lengthwise fracture in functionally graded single leg four-point bending beam configuration is performed. The material is functionally graded along the height as well as along the width of the beam. A lengthwise crack is located arbitrary along the beam height. The mechanical behaviour of beam is described by power-law stress-strain relation. The fracture is studied analytically in terms of the strain energy release rate. The solution derived is verfied by analysing the fracture with the help of the J-integral. The influences of crack location, material gradient along the height as well as along the width of beam and the non-linear behaviour of material on the fracture are investigated. It is found that the material non-linearity has to be taken into account in fracture mechanics based safety design of functionally graded structural members and components. The analysis revealed also that the strain energy release rate can be regulated effectively by employing appropriate material gradients in functionally graded structures.

1 Introduction

Functionally graded materials are extensively used for production of structural members and components which are subjected to non-uniform service requirements (Bohidar *et al*., 2014; Bykov *et al*., 2012; Butcher *et al*., 1999; Gasik, 2010; Hirai and Chen, 1999; Lu *et al.*, 2009; Mortensen and Suresh, 1995; Nemat-Allal *et al*., 2011; Neubrand and Rödel, 1997; Parvanova *et al*., 2013; Parvanova *et al*., 2014; Suresh and Mortensen, 1998; Tokova *et al*., 2016; Tokovyy and Ma, 2013; Tokovyy and Ma, 2016; Uslu Uysal and Kremzer, 2015; Uslu Uysal, 2016). This is due to the fact that these novel inhomogeneous materials possess continuously varying mechanical properties. The composition of constituent materials is changed gradually in one or more directions during manufacturing of a functionally graded structural member. Due to the smooth variation of macrostructure, the interfacial stress concentrations are largely avoided which is one of the most important advantages of functionally graded materials over the fibre reinforced composites (Szekrenyes, 2010; Szekrenyes and Vicente, 2012; Tkacheva, 2008).

Fracture is the most common failure mechanism in structural members made of functionally graded materials. Fracture can cause loss of stiffness and may lead to catastrophic failure. Thus, characterization of fracture behaviour is of great importance in the evaluation of functionally graded structures for durability and safety (Carpinteri and Pugno, 2006; Erdogan, 1995; Paulino, 2002; Szekrenyes, 2016; Szekrenyes, 2016; Shi-Dong Pan *et al*., 2009; Tilbrook *et al*., 2005; Upadhyay and Simha, 2007; Uslu Uysal and Güven, 2016).

The present paper addresses the problem of lengthwise fracture in two-dimensional functionally graded single leg four-point bending non-linear elastic beam. The fracture is studied in terms of the strain energy release rate. The solution derived is applied to elucidate the influence of crack location, material gradient along the height as well as along the width of beam and material non-linearity on the fracture behaviour.

2 Determination of the Strain Energy Release Rate

The single leg four-point bending beam configuration analyzed in the present paper is shown schematically in Figure 1. The beam is loaded by two external forces, F, applied symmetrically with respect to the mid-span. A

notch of depth, h_2, is cut in order to introduce conditions for lengthwise fracture. A lengthwise crack of length, *a*, is located arbitrary along the beam height (it should be mentioned that the present paper is motivated also by the fact that functionally graded materials can be built up layer by layer (Bohidar et al., 2014) which is a premise for appearance of lengthwise cracks between layers). The upper and lower crack arm have different thickness denoted by h_1 and h_2, respectively. It is obvious that the lower crack arm is free of stresses. It should be noted that the crack is located in the beam portion between the two external forces (obviously, this beam portion is loaded in pure bending). The beam has a rectangular cross-section of width, *b*, and height, 2*h*.

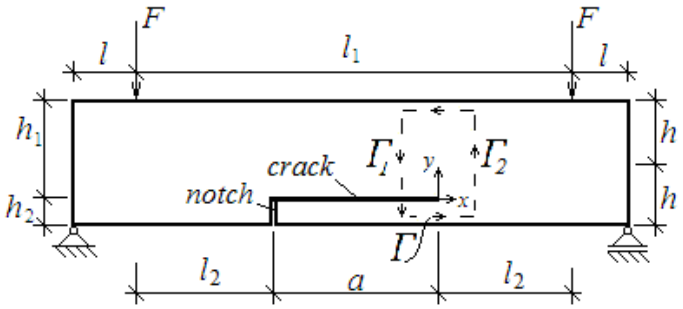

Figure 1. The geometry and loading of a functionally graded single leg four-point bending beam

The beam mechanical behaviour is described by a power-law stress-strain relation (Petrov, 2014)

$$\sigma = B\varepsilon^n, \tag{1}$$

where σ is the normal longitudinal stress, ε is the longitudinal strain, *B* and *n* are material properties. Stress-strain relation (1) describes non-linear elastic material behaviour which is typical for some functionally graded materials (for instance, zircona-titanium functionally graded material exhibits such behaviour at low content of zircona). The material behaviour of annealed copper and aluminium alloy can also be described by (1).

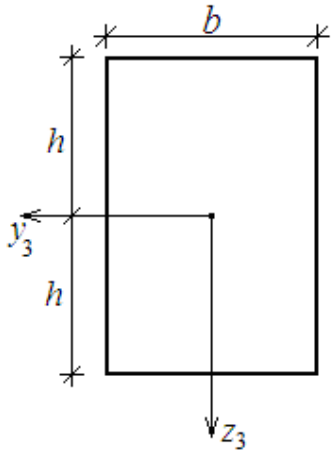

Figure 2. The beam cross-section

The material is functionally graded along the width as well as along the height of beam. The material property, *B*, varies continuously in the beam cross-section according to the following law:

$$B = B_U + \frac{B_L - B_U}{2h}(h + z_3) + \frac{64B_0}{b^6} y_3^6, \; -h \le z_3 \le h, \; -\frac{b}{2} \le y_3 \le \frac{b}{2}, \tag{2}$$

where B_U and B_L are, respectively, the values of *B* in the upper and lower surface of beam, B_0 is a material property that governs the material gradient along the beam width, y_3 and z_3 are the centroidal axes of beam cross-section (Figure 2). Formula (2) indicates that *B* is distributed symmetrically with respect to z_3-axis.

It should be noted that the fracture analysis developed in the present paper is based on the small strains assumption.

In order to derive the strain energy release rate, a small increase, Δa, of the crack length is assumed (the external load is kept constant). The strain energy release rate is written as

$$G = \frac{\Delta W_{ext} - \Delta U}{\Delta A}, \tag{3}$$

where the change of external work is

$$\Delta W_{ext} = \Delta U + \Delta U^{*}. \tag{4}$$

The increase of crack area is

$$\Delta A = b\Delta a. \tag{5}$$

In (3) and (4), ΔU and ΔU^{*} are the changes of strain energy and complementary strain energy, respectively. From (3), (4) and (5), it is found

$$G = \frac{\Delta U^{*}}{b\Delta a}, \tag{6}$$

where the change of complementary strain energy is

$$\Delta U^{*} = U_a^{*} - U_b^{*}. \tag{7}$$

In (7), U_a^{*} and U_b^{*} are the complementary strain energies after and before the increase of crack, respectively. Thus, G is written as

$$G = \frac{U_a^{*} - U_b^{*}}{b\Delta a}. \tag{8}$$

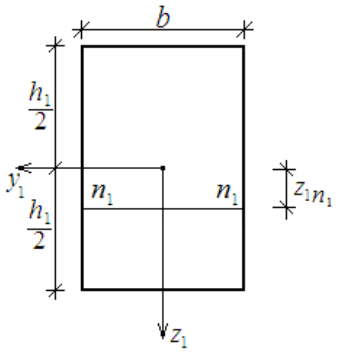

Figure 3. The upper crack arm cross-section ($n_1 - n_1$ is the neutral axis)

The complementary strain energy after the increase of crack is obtained by integrating the complementary strain energy density, u_0^{*}, in a portion of the upper crack arm (the lower crack arm is free of stresses) of length, Δa, behind the crack tip

$$U_a^* = \Delta a \int_{-\frac{h_1}{2}}^{\frac{h_1}{2}} \left(\int_{-\frac{b}{2}}^{\frac{b}{2}} u_0^* dy_1 \right) dz_1 , \tag{9}$$

where y_1 and z_1 are the centroidal axes of cross-section of the upper crack arm (Figure 3).

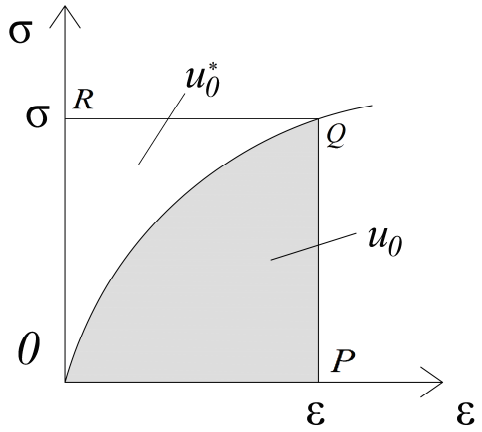

Figure 4. Non-linear stress-strain curve (u_0 and u_0^* are the strain energy density and complementary strain energy density, respectively)

The complementary strain energy density is equal to the area, *OQR*, which supplements the area, *OPQ*, enclosed by the stress-strain curve to a rectangle (Figure 4). Thus, u_0^* is written as

$$u_0^* = \sigma\varepsilon - u_0 . \tag{10}$$

The strain energy density, u_0, is equal to the area *OPQ* enclosed by the stress-strain curve (Figure 4). Thus,

$$u_0 = \int_0^{\varepsilon} \sigma(\varepsilon) d\varepsilon . \tag{11}$$

By combining of (1) and (11), it is found

$$u_0 = \frac{B\varepsilon^{n+1}}{n+1} . \tag{12}$$

By substituting of (1) and (12) in (10), it is derived

$$u_0^* = \frac{nB\varepsilon^{n+1}}{n+1} . \tag{13}$$

The strain, ε, which is necessary to calculate u_0^* is analyzed by applying the Bernoulli's hypothesis for plane sections, since the span to height ratio of the beam under consideration is large. Concerning the application of Bernoulli's hypothesis in the present paper, it can also be mentioned that the beam portion between the external forces is loaded in pure bending (Figure 1). Therefore, the only non-zero strain in this beam portion is ε. Thus, according to the small strain compatibility equations, ε is distributed linearly along the beam height

$$\varepsilon = \kappa_U (z_1 - z_{1n_1}) , \tag{14}$$

where κ_U and z_{1n_1} are the curvature and the neutral axis coordinate of upper crack arm (the neutral axis shifts from the centroid (Figure 3), since the material is functionally graded).

The curvature and the neutral axis coordinate are determined form the following equilibrium equations of upper crack arm cross-section:

$$N = \int_{-\frac{h_1}{2}}^{\frac{h_1}{2}} \left(\int_{-\frac{b}{2}}^{\frac{b}{2}} \sigma dy_1 \right) dz_1 , \tag{15}$$

$$M_{y_1} = \int_{-\frac{h_1}{2}}^{\frac{h_1}{2}} \left(\int_{-\frac{b}{2}}^{\frac{b}{2}} \sigma z_1 dy_1 \right) dz_1 , \tag{16}$$

where N and M_{y_1} are, respectively, the axial force and the bending moment in the upper crack arm. It is obvious that (Figure 1)

$$N = 0 , \; M_{y_1} = Fl . \tag{17}$$

In order to facilitate the integration in (15) and (16), the variation of B in the upper crack arm cross-section is expressed as (refer to (2))

$$B = B_U + \frac{B_{L1} - B_U}{h_1} \left(\frac{h_1}{2} + z_1 \right) + \frac{64 B_0}{b^6} y_1^6 , \tag{18}$$

where

$$B_{L1} = B_U + \frac{B_L - B_U}{2h} h_1 \tag{19}$$

is the value of B at the level of lengthwise crack.

By substituting of (1), (2), (14) and (18) in (15) and (16), it is obtained

$$\begin{aligned} 0 = {} & \frac{B_0}{7(n+1)} \left[\left(\frac{h_1}{2} - z_{1n_1} \right)^{n+1} - \left(-\frac{h_1}{2} - z_{1n_1} \right)^{n+1} \right] + \\ & + \frac{1}{n+1} \left[\frac{1}{2} (B_U + B_{L1}) + \frac{1}{h_1} (B_{L1} - B_U) z_{1n_1} \right] \left[\left(\frac{h_1}{2} - z_{1n_1} \right)^{n+1} - \left(-\frac{h_1}{2} - z_{1n_1} \right)^{n+1} \right] + \\ & + \frac{1}{h_1} (B_{L1} - B_U) \frac{1}{n+2} \left[\left(\frac{h_1}{2} - z_{1n_1} \right)^{n+2} - \left(-\frac{h_1}{2} - z_{1n_1} \right)^{n+2} \right] , \end{aligned} \tag{20}$$

$$M_{y_1} = b \kappa_U^n \left\{ \frac{B_0}{7(n+2)} \left[\left(\frac{h_1}{2} - z_{1n_1} \right)^{n+2} - \left(-\frac{h_1}{2} - z_{1n_1} \right)^{n+2} \right] + \right.$$

$$+\frac{B_0 z_{1n_1}}{7(n+1)}\left[\left(\frac{h_1}{2}-z_{1n_1}\right)^{n+1}-\left(-\frac{h_1}{2}-z_{1n_1}\right)^{n+1}\right]+$$

$$+B_U\left\{\frac{1}{n+2}\left[\left(\frac{h_1}{2}-z_{1n_1}\right)^{n+2}-\left(-\frac{h_1}{2}-z_{1n_1}\right)^{n+2}\right]+\right.$$

$$\left.+\frac{1}{n+1}\left[\left(\frac{h_1}{2}-z_{1n_1}\right)^{n+1}z_{1n_1}-\left(-\frac{h_1}{2}-z_{1n_1}\right)^{n+1}z_{1n_1}\right]\right\}+$$

$$+\frac{1}{2}\left(B_{L1}-B_U\right)\left\{\frac{1}{n+2}\left[\left(\frac{h_1}{2}-z_{1n_1}\right)^{n+2}-\left(-\frac{h_1}{2}-z_{1n_1}\right)^{n+2}\right]+\right.$$

$$\left.+\frac{z_{1n_1}}{n+1}\left[\left(\frac{h_1}{2}-z_{1n_1}\right)^{n+1}-\left(-\frac{h_1}{2}-z_{1n_1}\right)^{n+1}\right]\right\}+$$

$$+\frac{1}{h_1}\left(B_{L1}-B_U\right)\left\{\frac{1}{n+3}\left[\left(\frac{h_1}{2}-z_{1n_1}\right)^{n+3}-\left(-\frac{h_1}{2}-z_{1n_1}\right)^{n+3}\right]+\right.$$

$$+\frac{2z_{1n_1}}{n+2}\left[\left(\frac{h_1}{2}-z_{1n_1}\right)^{n+2}-\left(-\frac{h_1}{2}-z_{1n_1}\right)^{n+2}\right]+$$

$$\left.\left.+\frac{z_{1n_1}^2}{n+1}\left[\left(\frac{h_1}{2}-z_{1n_1}\right)^{n+1}-\left(-\frac{h_1}{2}-z_{1n_1}\right)^{n+1}\right]\right\}\right\}. \tag{21}$$

Apparently, at $n=1$ the non-linear stress-strain relation (1) transforms into the Hooke's law. This means that at $n=1$ equation (21) should transform in the formula for curvature of linear-elastic beam. Indeed, by substituting of at $n=1$, $B_U=B_L=E$ and $B_0=0$ (E is the modulus of elasticity) in (21), it is obtained

$$\kappa_U=\frac{12M_{y_1}}{Eb{h_1}^3}\ , \tag{22}$$

which is exact match of the formula for the curvature of linear-elastic homogeneous beam (Dowling, 2007). Equations (20) and (21) should be solved with respect to κ_U and z_{1n_1} by using the MatLab computer program.

By substituting of (13), (14) and (18) in (9) the complementary strain energy after the increase of crack length is derived as

$$U_a^*=b\Delta a\left\{\frac{\kappa_U^{n+1}B_0 n}{7(n+1)(n+2)}\left[\left(-\frac{h_1}{2}-z_{1n_1}\right)^{n+2}-\left(\frac{h_1}{2}-z_{1n_1}\right)^{n+2}\right]+\right.$$

$$+\frac{\kappa_U^{n+1}B_U}{(n+1)(n+2)}\left[\left(-\frac{h_1}{2}-z_{1n_1}\right)^{n+2}-\left(\frac{h_1}{2}-z_{1n_1}\right)^{n+2}\right]+$$

$$\left.+\frac{\kappa_U^{n+1}\left(B_{L1}-B_U\right)}{n+1}\left\{\frac{1}{2(n+2)}\left[\left(-\frac{h_1}{2}-z_{1n_1}\right)^{n+2}-\left(\frac{h_1}{2}-z_{1n_1}\right)^{n+2}\right]+\right.\right.$$

$$+\frac{1}{h_1(n+3)}\left[\left(-\frac{h_1}{2}-z_{1n_1}\right)^{n+3}-\left(\frac{h_1}{2}-z_{1n_1}\right)^{n+3}\right]+$$
$$+\frac{z_{1n_1}}{h_1(n+2)}\left[\left(-\frac{h_1}{2}-z_{1n_1}\right)^{n+2}-\left(\frac{h_1}{2}-z_{1n_1}\right)^{n+2}\right]\Bigg\}+$$
$$+\kappa_U^{n+1}\Bigg\{\frac{B_U}{n+2}\left[\left(\frac{h_1}{2}-z_{1n_1}\right)^{n+2}-\left(-\frac{h_1}{2}-z_{1n_1}\right)^{n+2}\right]+$$
$$+\frac{B_{L1}-B_U}{2(n+2)}\left[\left(\frac{h_1}{2}-z_{1n_1}\right)^{n+2}-\left(-\frac{h_1}{2}-z_{1n_1}\right)^{n+2}\right]+$$
$$+\frac{B_{L1}-B_U}{h_1(n+3)}\left[\left(\frac{h_1}{2}-z_{1n_1}\right)^{n+3}-\left(-\frac{h_1}{2}-z_{1n_1}\right)^{n+3}\right]+$$
$$+\frac{z_{1n_1}(B_{L1}-B_U)}{h_1(n+2)}\left[\left(\frac{h_1}{2}-z_{1n_1}\right)^{n+2}-\left(-\frac{h_1}{2}-z_{1n_1}\right)^{n+2}\right]\Bigg\}\Bigg\}, \tag{23}$$

where κ_U and z_{1n_1} are determined from equations (20) and (21).

The complementary strain energy, U_b^*, before the increase of crack length is determined by integrating the complementary strain energy density in a beam portion of length, Δa, ahead of the crack tip. Obviously, U_b^* can be obtained by applying formula (23). For this purpose, h_1, κ_U and z_{1n_1} should be replaced with $2h$, κ and z_{3n_3}, respectively (κ and z_{3n_3} are the curvature and the coordinate of neutral axis of cross-section of un-cracked beam portion ahead of the crack tip). The same replacements should be done in equilibrium equations (20) and (21) in order to determine κ and z_{3n_3}. Besides, h_1 should be replaced with $2h$ in (19).

By substituting of U_a^* and U_b^* in (8), it is derived

$$G=\frac{\kappa_U^{n+1}B_0 n}{7(n+1)(n+2)}\left[\left(-\frac{h_1}{2}-z_{1n_1}\right)^{n+2}-\left(\frac{h_1}{2}-z_{1n_1}\right)^{n+2}\right]+$$
$$+\frac{\kappa_U^{n+1}B_U}{(n+1)(n+2)}\left[\left(-\frac{h_1}{2}-z_{1n_1}\right)^{n+2}-\left(\frac{h_1}{2}-z_{1n_1}\right)^{n+2}\right]+$$
$$+\frac{\kappa_U^{n+1}(B_{L1}-B_U)}{n+1}\Bigg\{\frac{1}{2(n+2)}\left[\left(-\frac{h_1}{2}-z_{1n_1}\right)^{n+2}-\left(\frac{h_1}{2}-z_{1n_1}\right)^{n+2}\right]+$$
$$+\frac{1}{h_1(n+3)}\left[\left(-\frac{h_1}{2}-z_{1n_1}\right)^{n+3}-\left(\frac{h_1}{2}-z_{1n_1}\right)^{n+3}\right]+$$
$$+\frac{z_{1n_1}}{h_1(n+2)}\left[\left(-\frac{h_1}{2}-z_{1n_1}\right)^{n+2}-\left(\frac{h_1}{2}-z_{1n_1}\right)^{n+2}\right]\Bigg\}+$$

$$
\begin{aligned}
&+\kappa_U^{\,n+1}\left\{\frac{B_U}{n+2}\left[\left(\frac{h_1}{2}-z_{1n_1}\right)^{n+2}-\left(-\frac{h_1}{2}-z_{1n_1}\right)^{n+2}\right]+\right.\\
&+\frac{B_{L1}-B_U}{2(n+2)}\left[\left(\frac{h_1}{2}-z_{1n_1}\right)^{n+2}-\left(-\frac{h_1}{2}-z_{1n_1}\right)^{n+2}\right]+\\
&+\frac{B_{L1}-B_U}{h_1(n+3)}\left[\left(\frac{h_1}{2}-z_{1n_1}\right)^{n+3}-\left(-\frac{h_1}{2}-z_{1n_1}\right)^{n+3}\right]+\\
&\left.+\frac{z_{1n_1}(B_{L1}-B_U)}{h_1(n+2)}\left[\left(\frac{h_1}{2}-z_{1n_1}\right)^{n+2}-\left(-\frac{h_1}{2}-z_{1n_1}\right)^{n+2}\right]\right\}-\\
&-\left\{\frac{\kappa^{n+1}B_0 n}{7(n+1)(n+2)}\left[\left(-h-z_{3n_3}\right)^{n+2}-\left(h-z_{3n_3}\right)^{n+2}\right]+\right.\\
&+\frac{\kappa^{n+1}B_U}{(n+1)(n+2)}\left[\left(-h-z_{3n_3}\right)^{n+2}-\left(h-z_{3n_3}\right)^{n+2}\right]+\\
&+\frac{\kappa^{n+1}(B_L-B_U)}{n+1}\left\{\frac{1}{2(n+2)}\left[\left(-h-z_{3n_3}\right)^{n+2}-\left(h-z_{3n_3}\right)^{n+2}\right]+\right.\\
&+\frac{1}{2h(n+3)}\left[\left(-h-z_{3n_3}\right)^{n+3}-\left(h-z_{3n_3}\right)^{n+3}\right]+\\
&\left.+\frac{z_{3n_3}}{2h(n+2)}\left[\left(-h-z_{3n_3}\right)^{n+2}-\left(h-z_{3n_3}\right)^{n+2}\right]\right\}+\\
&+\kappa^{n+1}\left\{\frac{B_U}{n+2}\left[\left(h-z_{3n_3}\right)^{n+2}-\left(-h-z_{3n_3}\right)^{n+2}\right]+\right.\\
&+\frac{B_L-B_U}{2(n+2)}\left[\left(h-z_{3n_3}\right)^{n+2}-\left(-h-z_{3n_3}\right)^{n+2}\right]+\\
&+\frac{B_L-B_U}{2h(n+3)}\left[\left(h-z_{3n_3}\right)^{n+3}-\left(-h-z_{3n_3}\right)^{n+3}\right]+\\
&\left.\left.+\frac{z_{3n_3}(B_L-B_U)}{2h(n+2)}\left[\left(h-z_{3n_3}\right)^{n+2}-\left(-h-z_{3n_3}\right)^{n+2}\right]\right\}\right\}. \qquad (24)
\end{aligned}
$$

Formula (24) calculates the strain energy release rate for the two-dimensional functionally graded single leg four-point bending configuration (Figure 1) when the mechanical behaviour of beam and the variation of material property, *B*, in the beam cross-section are described by formulae (1) and (2), respectively. It should be noted that at $n=1$, $B_U=B_L=E$, $B_0=0$ and $h_1=h$ formula (24) transforms in

$$
G=\frac{21F^2l^2}{4Eb^2h^3}, \qquad (25)
$$

which is exact match of the expression for strain energy release rate in linear-elastic homogeneous single leg four-point bending configuration when the delamination crack is located in the beam mid-plane (Hutchinson and Suo, 1992).

In order to verify (24), an additional non-linear elastic analysis of the lengthwise fracture is performed by applying the *J*-integral approach (Broek, 1986)

$$J = \int_{\Gamma} \left[u_0 \cos\alpha - \left(p_x \frac{\partial u}{\partial x} + p_y \frac{\partial v}{\partial x} \right) \right] ds \,, \tag{26}$$

where Γ is a contour of integration going from the lower crack face to the upper crack face in the counter clockwise direction, α is the angle between the outwards normal vector to the contour of integration and the crack direction, p_x and p_y are the components of stress vector, *u* and *v* are the components of displacement vector with respect to the crack tip coordinate system *xy* (*x* is directed along the crack), *ds* is a differential element along the contour.

The integration is carried-out by using the integration contour, Γ, which is shown with dotted line in Figure 1. Obviously, the *J*-integral is non-zero only in segments Γ_1 and Γ_2. Thus, the *J*-integral solution is written as

$$J = J_{\Gamma_1} + J_{\Gamma_2} \,, \tag{27}$$

where J_{Γ_1} and J_{Γ_2} are the *J*-integral values in segments Γ_1 and Γ_2, respectively. The *J*-integral components in segment Γ_1 (this segment coincides with the cross-section of the upper crack arm) are written as

$$p_x = -\sigma = -B\varepsilon^n,\ p_y = 0,\ ds = dz_1,\ \cos\alpha = -1,\ \frac{\partial u}{\partial x} = \varepsilon = \kappa_U \left(z_1 - z_{1n_1} \right), \tag{28}$$

where z_1 varies in the interval $[-h_1/2,\ h_1/2]$. By substituting of (12), (18) and (28) in (26) and integrating in boundaries from $-h_1/2$ to $h_1/2$, it is obtained

$$\begin{aligned}
J_{\Gamma_1} = {} & \frac{64\kappa_U^{n+1} B_0 n y_1^6}{b^6 (n+1)(n+2)} \left[\left(-\frac{h_1}{2} - z_{1n_1} \right)^{n+2} - \left(\frac{h_1}{2} - z_{1n_1} \right)^{n+2} \right] + \\
& + \frac{\kappa_U^{n+1} B_U}{(n+1)(n+2)} \left[\left(-\frac{h_1}{2} - z_{1n_1} \right)^{n+2} - \left(\frac{h_1}{2} - z_{1n_1} \right)^{n+2} \right] + \\
& + \frac{\kappa_U^{n+1} (B_{L1} - B_U)}{n+1} \left\{ \frac{1}{2(n+2)} \left[\left(-\frac{h_1}{2} - z_{1n_1} \right)^{n+2} - \left(\frac{h_1}{2} - z_{1n_1} \right)^{n+2} \right] + \right. \\
& \quad + \frac{1}{h_1 (n+3)} \left[\left(-\frac{h_1}{2} - z_{1n_1} \right)^{n+3} - \left(\frac{h_1}{2} - z_{1n_1} \right)^{n+3} \right] + \\
& \quad \left. + \frac{z_{1n_1}}{h_1 (n+2)} \left[\left(-\frac{h_1}{2} - z_{1n_1} \right)^{n+2} - \left(\frac{h_1}{2} - z_{1n_1} \right)^{n+2} \right] \right\} + \\
& + \kappa_U{}^{n+1} \left\{ \frac{B_U}{n+2} \left[\left(\frac{h_1}{2} - z_{1n_1} \right)^{n+2} - \left(-\frac{h_1}{2} - z_{1n_1} \right)^{n+2} \right] + \right. \\
& \quad \left. + \frac{B_{L1} - B_U}{2(n+2)} \left[\left(\frac{h_1}{2} - z_{1n_1} \right)^{n+2} - \left(-\frac{h_1}{2} - z_{1n_1} \right)^{n+2} \right] + \right.
\end{aligned}$$

$$+\frac{B_{L1}-B_U}{h_1(n+3)}\left[\left(\frac{h_1}{2}-z_{1n_1}\right)^{n+3}-\left(-\frac{h_1}{2}-z_{1n_1}\right)^{n+3}\right]+$$
$$+\frac{z_{1n_1}(B_{L1}-B_U)}{h_1(n+2)}\left[\left(\frac{h_1}{2}-z_{1n_1}\right)^{n+2}-\left(-\frac{h_1}{2}-z_{1n_1}\right)^{n+2}\right]\Bigg\}, \tag{29}$$

where y_1 varies in the interval $[-b/2,\, b/2]$. Formula (29) can be used also to obtain the *J*-integral solution in segment, Γ_2, of the integration contour (Figure 1). For this purpose, h_1, κ_U and z_{1n_1} should be replaced with $2h$, κ and z_{3n_3}, respectively. Besides, the sign of (29) must be set to „minus" because the integration contour is directed upwards in segment, Γ_2. Finally, J_{Γ_1} and J_{Γ_2} are substituted in (27)

$$J=\frac{64\kappa_U^{n+1}B_0ny_1^6}{b^6(n+1)(n+2)}\left[\left(-\frac{h_1}{2}-z_{1n_1}\right)^{n+2}-\left(\frac{h_1}{2}-z_{1n_1}\right)^{n+2}\right]+$$
$$+\frac{\kappa_U^{n+1}B_U}{(n+1)(n+2)}\left[\left(-\frac{h_1}{2}-z_{1n_1}\right)^{n+2}-\left(\frac{h_1}{2}-z_{1n_1}\right)^{n+2}\right]+$$
$$+\frac{\kappa_U^{n+1}(B_{L1}-B_U)}{n+1}\Bigg\{\frac{1}{2(n+2)}\left[\left(-\frac{h_1}{2}-z_{1n_1}\right)^{n+2}-\left(\frac{h_1}{2}-z_{1n_1}\right)^{n+2}\right]+$$
$$+\frac{1}{h_1(n+3)}\left[\left(-\frac{h_1}{2}-z_{1n_1}\right)^{n+3}-\left(\frac{h_1}{2}-z_{1n_1}\right)^{n+3}\right]+$$
$$+\frac{z_{1n_1}}{h_1(n+2)}\left[\left(-\frac{h_1}{2}-z_{1n_1}\right)^{n+2}-\left(\frac{h_1}{2}-z_{1n_1}\right)^{n+2}\right]\Bigg\}+$$
$$+\kappa_U^{n+1}\Bigg\{\frac{B_U}{n+2}\left[\left(\frac{h_1}{2}-z_{1n_1}\right)^{n+2}-\left(-\frac{h_1}{2}-z_{1n_1}\right)^{n+2}\right]+$$
$$+\frac{B_{L1}-B_U}{2(n+2)}\left[\left(\frac{h_1}{2}-z_{1n_1}\right)^{n+2}-\left(-\frac{h_1}{2}-z_{1n_1}\right)^{n+2}\right]+$$
$$+\frac{B_{L1}-B_U}{h_1(n+3)}\left[\left(\frac{h_1}{2}-z_{1n_1}\right)^{n+3}-\left(-\frac{h_1}{2}-z_{1n_1}\right)^{n+3}\right]+$$
$$+\frac{z_{1n_1}(B_{L1}-B_U)}{h_1(n+2)}\left[\left(\frac{h_1}{2}-z_{1n_1}\right)^{n+2}-\left(-\frac{h_1}{2}-z_{1n_1}\right)^{n+2}\right]\Bigg\}-$$
$$-\Bigg\{\frac{64\kappa^{n+1}B_0ny_1^6}{b^6(n+1)(n+2)}\left[\left(-h-z_{3n_3}\right)^{n+2}-\left(h-z_{3n_3}\right)^{n+2}\right]+$$
$$+\frac{\kappa^{n+1}B_U}{(n+1)(n+2)}\left[\left(-h-z_{3n_3}\right)^{n+2}-\left(h-z_{3n_3}\right)^{n+2}\right]+$$
$$+\frac{\kappa^{n+1}(B_L-B_U)}{n+1}\Bigg\{\frac{1}{2(n+2)}\left[\left(-h-z_{3n_3}\right)^{n+2}-\left(h-z_{3n_3}\right)^{n+2}\right]+$$

$$+\frac{1}{2h(n+3)}\left[\left(-h-z_{3n_3}\right)^{n+3}-\left(h-z_{3n_3}\right)^{n+3}\right]+$$
$$+\frac{z_{3n_3}}{2h(n+2)}\left[\left(-h-z_{3n_3}\right)^{n+2}-\left(h-z_{3n_3}\right)^{n+2}\right]\Bigg\}+$$
$$+\kappa^{n+1}\Bigg\{\frac{B_U}{n+2}\left[\left(h-z_{3n_3}\right)^{n+2}-\left(-h-z_{3n_3}\right)^{n+2}\right]+$$
$$+\frac{B_L-B_U}{2(n+2)}\left[\left(h-z_{3n_3}\right)^{n+2}-\left(-h-z_{3n_3}\right)^{n+2}\right]+$$
$$+\frac{B_L-B_U}{2h(n+3)}\left[\left(h-z_{3n_3}\right)^{n+3}-\left(-h-z_{3n_3}\right)^{n+3}\right]+$$
$$+\frac{z_{3n_3}\left(B_L-B_U\right)}{2h(n+2)}\left[\left(h-z_{3n_3}\right)^{n+2}-\left(-h-z_{3n_3}\right)^{n+2}\right]\Bigg\}\Bigg\}. \tag{30}$$

It should be mentioned that formula (30) describes the distribution of the *J*-integral value along the crack front. The average value of the *J*-integral along the crack front is expressed as

$$J_{av}=\frac{1}{b}\int_{-\frac{b}{2}}^{\frac{b}{2}} J\,dy_1\ . \tag{31}$$

The formula derived by substituting of (30) in (31) is exact match of (24). This fact is a verification of the fracture analysis developed in the present paper.

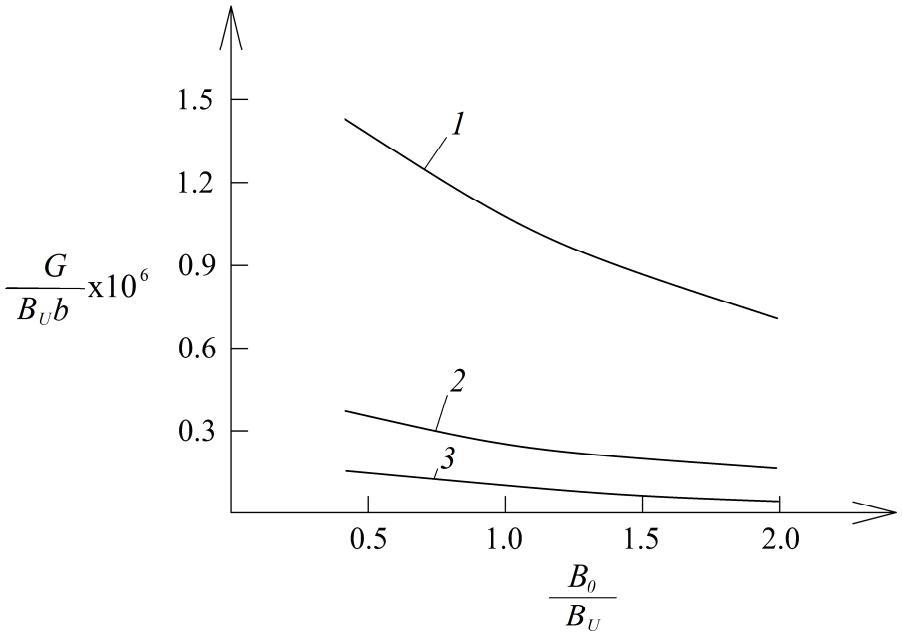

Figure 5. The strain energy release rate in non-dimensional form plotted against B_0 / B_U ratio (curve 1 – for $h_1 / 2h = 0.25$, curve 2 - for $h_1 / 2h = 0.50$ and curve 3 - for $h_1 / 2h = 0.75$)

The influence of lengthwise crack position along the height of beam cross-section, the material gradient along the height as well as along width of beam and material non-linearity on the fracture behaviour of functionally graded

single leg four-point bending beam is investigated. For this purpose, calculations of the strain energy release rate are performed by using formula (24). It is assumed that b=0.02 m, h=0.005 m, l=0.1 m and F=50 N. The strain energy release rate is presented in non-dimensional form by using the formula, $G_N = G/(B_U b)$. The crack location along the height of beam cross-section is characterized by $h_1/2h$ ratio. The material gradients along the beam width and along beam height are characterized by B_0/B_U and B_L/B_U ratios, respectively. The strain energy release rate is plotted in non-dimensional form against B_0/B_U ratio at $B_L/B_U = 0.5$ and n=0.8 for three $h_1/2h$ ratios in Figure 5. It should be noted that in the calculations B_U is kept constant (thus, B_0 is varied in order to generate various B_0/B_U ratios). The curves in Figure 5 indicate that the strain energy release rate decreases with increasing of B_0/B_U ratio (this is due to the increase of beam stiffness). It can also be observed in Figure 5 that the strain energy release rate decreases with increasing of $h_1/2h$ ratio. This finding is attributed to the increase of the upper crack arm stiffness (the lower crack arm is free of stresses).

The effect of material gradient along the beam height is evaluated too. For this purpose, the strain energy release rate is presented as a function of B_L/B_U ratio at $h_1/2h = 0.25$ and $B_0/B_U = 0.8$ in Figure 6. One can observe that the strain energy release rate decreases with increasing of B_L/B_U ratio (Figure 6). The influence of non-linear behaviour of material on the fracture is also analyzed. The strain energy release rate obtained assuming linear-elastic behaviour of the functionally graded single leg four-point bending beam is plotted against B_L/B_U ratio in Figure 6 for comparison with the non-linear elastic solution (it should be mentioned that the linear-elastic solution is derived by substituting of n=1 in formula (24)).

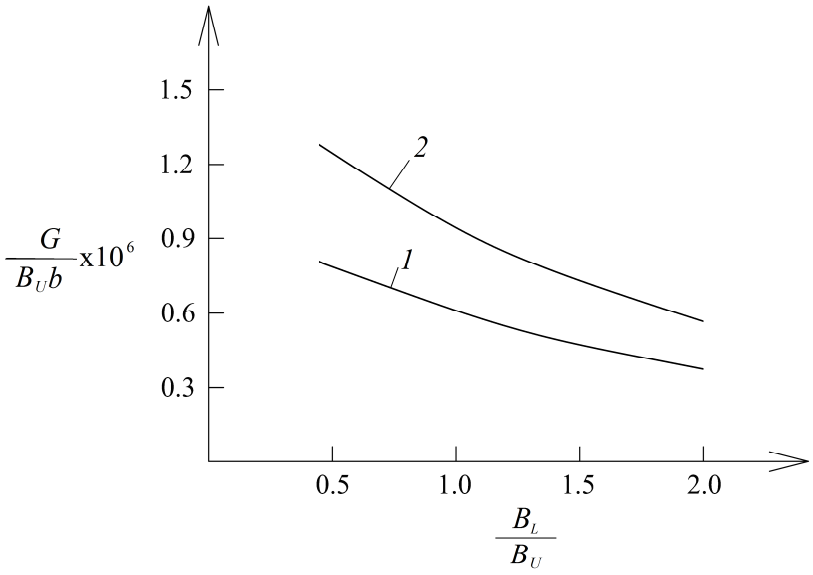

Figure 6. The strain energy release rate in non-dimensional form presented as a function of B_L/B_U ratio (curve 1 – linear-elastic behaviour of material, curve 2 – non-linear elastic behaviour)

It can be observed in Figure 6 that the material non-linearity leads to increase of the strain energy release rate.

3 Conclusions

A non-linear elastic fracture analysis of two-dimensional functionally graded single leg four-point bending beam configuration is performed. A lengthwise crack is located arbitrary along the height of beam cross-section. The fracture is studied analytically in terms of the strain energy release rate by using a power-law stress-strain relation. The material is functionally graded along the width as well as along the height of beam cross-section. The effects of crack location, material gradient and non-linear behaviour of material on the fracture are

elucidated. It is found that the strain energy release rate decreases with increasing of B_0 / B_U and B_L / B_U ratios (this finding indicates that the strain energy release rate can be regulated effectively by employing appropriate material gradients in the design stage of functionally graded structures). The analysis revealed also that the strain energy release rate decreases with increasing of the upper crack arm thickness. Since the non-linear behaviour of material leads to increase of the strain energy release rate, the material non-linearity has to be taken into account for an efficient and safe design of structural members and components made of two-dimensional functionally graded materials.

References

Bohidar, S.K.; Sharma, R.; Mishra, P.R.: Functionally graded materials: A critical review. *International Journal of Research*, 1, (2014), 289-301.

Broek, D.: *Elementary engineering fracture mechanics*. Springer (1986).

Butcher, R.J.; Rousseau, C.E.; Tippur, H.V.: A functionally graded particulate composite: Measurements and Failure Analysis. *Acta. Mater.*, 47, (1999), 259-268.

Bykov, Yu. V.; Egorov, S. V.; Ermeev, A. G.; Holoptsev, V. V.: Fabrication of metal-ceramic functionally graded materials by microwave sintering. Inorganic Materials: *Applied Research*, 3, (2012), DOI: 10.1134/S20751133120300057.

Carpinteri, A.; Pugno, N.: Cracks in re-entrant corners in functionally graded materials. *Engineering Fracture Mechanics*, 73, (2006), 1279-1291.

Dowling, N.: *Mechanical Behavior of Materials*. Pearson (2007).

Erdogan, F.: Fracture mechanics of functionally graded materials. *Comp. Eng.,* 5, (1995), 753-770.

Gasik, M.M.: Functionally graded materials: bulk processing techniques. *International Journal of Materials and Product Technology*, 39, (2010), 20-29.

Hirai, T.; Chen, L.: Recent and prospective development of functionally graded materials in Japan. *Mater Sci. Forum*, 308-311, (1999), 509-514.

Hutchinson, W.; Suo, Z.: Mixed mode cracking in layered materials. *Advances in Applied Mechanic*, 64, (1992), 804–810.

Lu, C.F.; Lim, C.W.; Chen, W.Q.: Semi-analytical analysis for multi-dimensional functionally graded plates: 3-D elasticity solutions. *Int. J. Num. Meth. Engng.,* 79, 2009, 25-44.

Mortensen, A.; Suresh, S.: Functionally graded metals and metal-ceramic composites: Part 1 *Processing. Int. Mater. Rev.*, 40, (1995), 239-265.

Nemat-Allal, M.M.; Ata, M.H.; Bayoumi, M.R,; Khair-Eldeen, W.: Powder metallurgical fabrication and microstructural investigations of Aluminum/Steel functionally graded material. *Materials Sciences and Applications*, 2, (2011), 1708-1718.

Neubrand, A.; Rödel, J.: Gradient materials: An overview of a novel concept. *Zeit f Met*, 88, (1997), 358-371.

Parvanova, S.L.; Dineva, P.S.; Manolis, G.D.: Dynamic behavior of a finite-sized elastic solid with multiple cavities and inclusions using BIEM. *Acta Mech*., 224, (2013), 597-618.

Parvanova, S.L.; Dineva, P.S.; Manolis, G.D.; Kochev, P.N.: Dynamic response of a solid with multiple inclusions under anti-plane strain conditions by the BEM. *Computers and Structures*, 139, (2014), 65-83.

Paulino, G.C.: Fracture in functionally graded materials. *Engng. Fract. Mech*, 69, (2002), 1519-1530.

Petrov, V.V.: Non-linear incremental structural mechanics. M.: *Infra-Injeneria* (2014).

Shi-Dong Pan; Ji-Cai Feng; Zhen-Gong Zhou; Wu-Lin-Zhi: Four parallel non-symetric Mode –III cracks with different lengths in a functionally graded material plane. *Strength, Fracture and Complexity*: an International Journal, 5, (2009), 143-166.

Suresh, S.; Mortensen, A.: *Fundamentals of functionally graded materials*. London: IOM Communications Ltd (1998).

Szekrenyes, A.: Fracture analysis in the modified split-cantilever beam using the classical theories of strength of materials. *Journal of Physics*: Conference Series, 240, (2010), 012030.

Szekrenyes, A.; Vicente, W.M.: Interlaminar fracture analysis in the GII-GIII plane using prestressed transparent composite beams. Composites Part A: *Applied Science and Manufacturing*, 43, (2012), 95-103.

Szekrenyes, A.: Semi-layerwise analysis of laminated plates with nonsingular delamination-The theorem of autocontinuity. *Applied Mathematical Modelling*, 40, (2016), 1344 – 1371.

Szekrenyes, A.: Nonsingular crack modelling in orthotropic plates by four equivalent single layers. *European Journal of Mechanic*s – A/solids, 55, (2016), 73-99.

Tilbrook, M.T.; Moon, R.J.; Hoffman, M.: Crack propagation in graded composites. *Composite Science and Technology*, 65, (2005), 201-220.

Tkacheva, L.A.: Unsteady crack propagation in the beam approximation. *Applied Mechanics and Technical Physics*, 49, (2008), 177 – 189.

Tokova, L.; Yasinskyy, A.; Ma, C.-C: Effect of the layer inhomogeneity on the distribution of stresses and displacements in an elastic multilayer cylinder. *Acta Mechanica*, (2016), DOI: 10.1007/s00707-015-1519-8, 1 – 13.

Tokovyy, Y.; Ma, C.-C: Three-Dimensional Temperature and Thermal Stress Analysis of an Inhomogeneous Layer., *Journal of Thermal Stresses*, 36, (2013), 790 – 808, DOI: 10.1080/01495739.2013.787853.

Tokovyy, Y.; Ma, C.-C: Axisymmetric Stresses in an Elastic Radially Inhomogeneous Cylinder Under Length-Varying Loadings. *ASME Journal of Applied Mechanics*, 83, (2016), DOI: 10.1115/1.4034459.

Upadhyay, A.K.; Simha, K.R.Y.: Equivalent homogeneous variable depth beams for cracked FGM beams; compliance approach. *Int. J. Fract.,* 144, (2007), 209-213.

Uslu Uysal, M.; Kremzer, M.: Buckling Behaviour of Short Cylindrical Functionally Gradient Polymeric Materials. *Acta Physica Polonica* A, 127, (2015), 1355-1357, DOI:10.12693/APhysPolA.127.1355.

Uslu Uysal, M.: Buckling behaviours of functionally graded polymeric thin-walled hemispherical shells. *Steel and Composite Structures*, an International Journal, 21, (2016), 849-862.

Uslu Uysal, M.; Güven, U.: A Bonded Plate Having Orthotropic Inclusion in Adhesive Layer under In-Plane Shear Loading. *The Journal of Adhesion*, 92, (2016), 214-235, DOI:10.1080/00218464.2015.1019064.

Address: Prof. Dr. Victor Rizov, Department of Technical Mechanics, University of Architecture, Civil Engineering and Geodesy, 1 Chr. Smirnensky blvd., 1046 – Sofia, Bulgaria.
email: V_RIZOV_FHE@UACG.BG